Electronic Supplementary Material (ESI) for Inorganic Chemistry Frontiers.

Surface-dynamic approach toward supercrystal engineering of titanium–oxo cluster

Ling-Cui Meng#, Zhi-Ming Feng#, Zhan-Guo Jiang*, and Cai-Hong Zhan*

Powder X-ray Diffraction (PXRD)

Powder XRD patterns were obtained using a Bruker D8 Advance X-ray diffractometer with (λ (CuKα) = 1.5405 Å) radiation.

Fourier Transform Infrared Spectroscopy (FTIR)

The materials were recorded on KBr disk using a Nicolet NEXUS 670 spectrometer between 400 and 4000 cm^{-1}.

Thermogravimetric Analyses (TGA)

They were carried out on a TA Instruments STA499 F5 thermobalance with a 100 $mL \cdot min^{-1}$ flow of nitrogen; the temperature was ramped from 20 °C to 800 °C at a rate of 10 $°C \cdot min^{-1}$.

Single-crystal X-ray Diffraction (SCXRD)

A suitable crystal of $(Ti_{10}Cu_2)_{sp}$ and $(Ti_{10}Cu_2)_{cs}$ were mounted in a Hampton cryoloop with Paratone® N oil cryoprotectant. Intensity data collections were carried out at T = 150 K with a Bruker D8 VENTURE diffractometer equipped with a PHOTON 100 CMOS bidimensional detector using a high brilliance IμS microfocus X-ray Mo Ka monochromatized radiation (λ = 0.71073 Å) and Cu Ka monochromatized radiation (λ = 1.54178 Å). With the aid of Olex2, the structure was solved with the ShelXT structure solution program using Intrinsic Phasing and refined with the ShelXL refinement package using Least Squares minimization. Further details about of the crystal structure determinations may be obtained free of charge via the Internet at https://www.ccdc.cam.ac.uk/ CCDC 2277134 and 2277142.

UV-Vis absorption spectra (UV)

Solid state UV-Vis absorption spectra were acquired on a Carry 5000 spectrophotometer, in which the range of wavenumber was setted at 200 to 800 nm.
Liquid UV absorption spectra were acquired on UV-5000PC (METASH), in which the range of wavenumber was setted at 250 to 800 nm.

Cyclic Voltammetry (CV)

Cyclic voltammetry (CV) experiments were carried out at room temperature in $CHCl_3$ on an electrochemical station (CHI 660E, China). All CV experiments were performed

using a glassy carbon (GC) electrode with a diameter of 3 mm as the working electrode. The electrode surface was polished routinely with 0.05 μm alumina–water slurry on a felt surface immediately before use. The counter electrode was a Pt wire and the reference electrode was a Ag/AgCl (KCl-saturated).

Linear sweep voltammetry (LSV)

Linear sweep voltammetry (LSV) experiments were carried out at room temperature on an electrochemical station (CHI 660E, China). The two crystals were ground to a thickness of 0.07 cm and a diameter of 0.8 cm, and then copper wires were fixed to the crystals using conductive silver glue. The samples were left overnight for testing.

Materials and reagents

All starting materials and regents were purchased from commercial suppliers and used without further purification. salicylic acid and $Ti(O^iPr)_4$ were purchased from Energy Chemical. $CuCl_2{\cdot}2H_2O$ (AR), and CH_3OH (AR) were purchased from Sinopharm Chemical Reagent Co., Ltd., China.

Synthesis and Experimental Section.

The synthesis of $[H_4Ti_{10}Cu_2(\mu_2\text{-}O)_6(\mu_3\text{-}O)_2(sal)_8(OCH_3)_{16}]$ $(Ti_{10}Cu_2)_{cs}$:

A total of 17.1 mg of $CuCl_2{\cdot}2H_2O$ (0.1 mmol), 27.6 mg of salicylic acid (0.2 mmol), and 4 mL of CH_3OH were mixed in a 20 mL glass bottle, and then 31 μL of $Ti(O^iPr)_4$ (0.1 mmol) was added. The solution was sonicated for 5 min and then transferred to an oven at 60 °C for 3 days. After cooling, green crystals were obtained, washed with EtOH, and then dried at room temperature (yield ~40%).

The synthesis of $[H_6Ti_{10}Cu_2(\mu_2\text{-}O)_6(\mu_3\text{-}O)_2(sal)_8\ (OCH_3)_{18}]$ $(Ti_{10}Cu_2)_{sp}$:

A total of 34.2 mg of $CuCl_2{\cdot}2H_2O$ (0.2 mmol), 55.2 mg of salicylic acid (0.4 mmol), and 8 mL of CH_3OH were mixed in a 20 mL glass bottle, and then 62 μL of $Ti(O^iPr)_4$ (0.2 mmol) was added. The solution was sonicated for 5 min and then transferred to an oven at 60 °C for 2 days. After cooling, yellow crystals were obtained, washed with EtOH, and then dried at room temperature (yield ~60%).

Structure

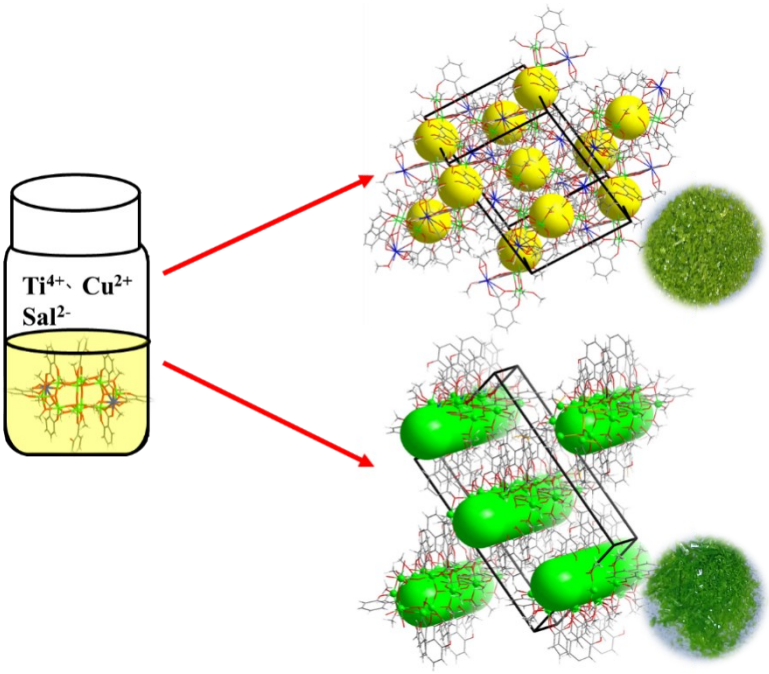

Figure S1. Schematic illustration of the crystallization.

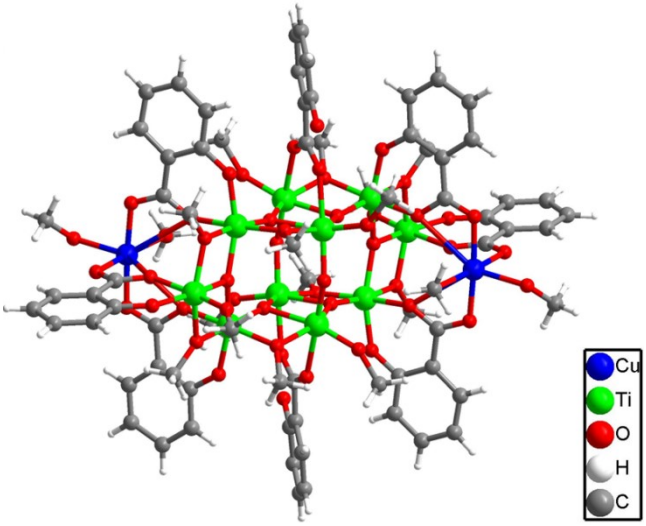

Figure S2. The structure of the $(Ti_{10}Cu_2)_{sp}$.

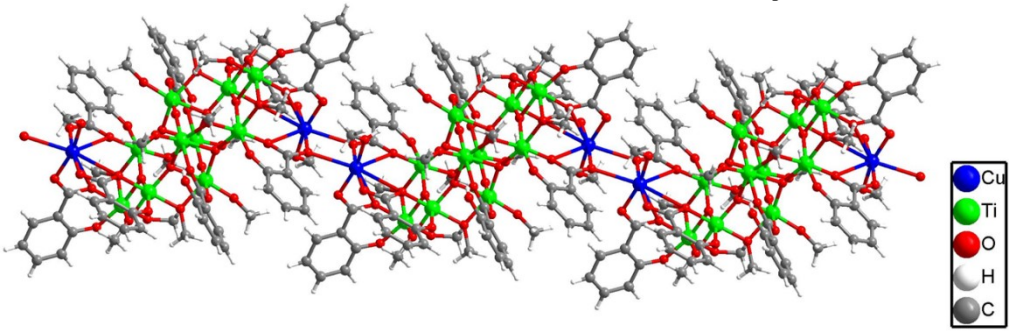

Figure S3. The structure of the $(Ti_{10}Cu_2)_{cs}$.

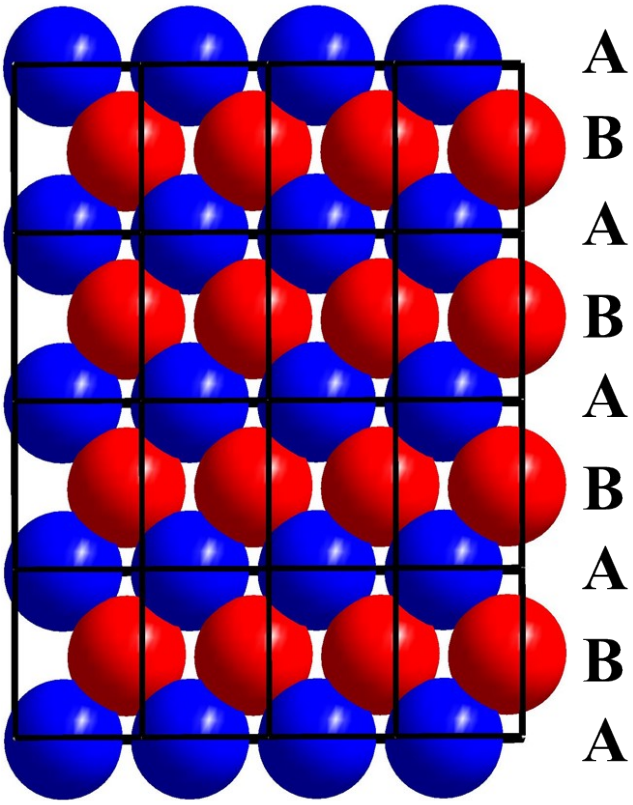

Figure S4. The ABAB stacking in $(Ti_{10}Cu_2)_{sp}$.

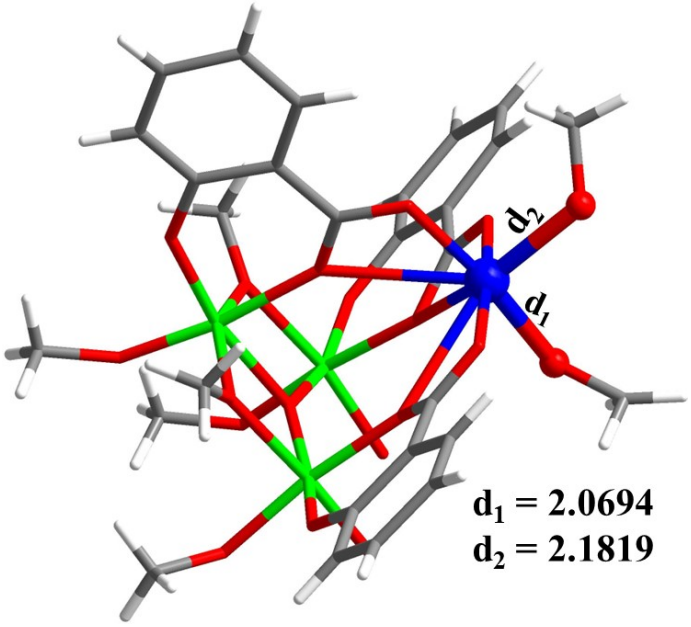

Figure S5. The bond lengths (Å) of relative Cu-O in $(Ti_{10}Cu_2)_{sp}$.

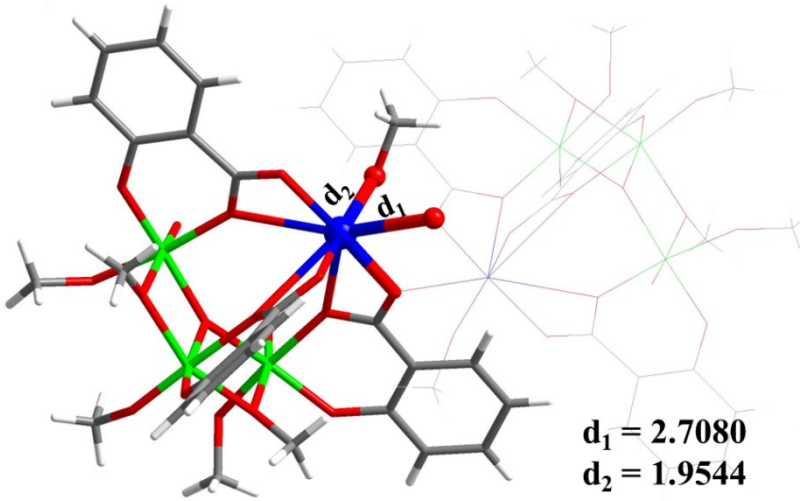

Figure S6. The bond lengths (Å) of relative Cu-O in $\mathbf{(Ti_{10}Cu_2)_{cs}}$.

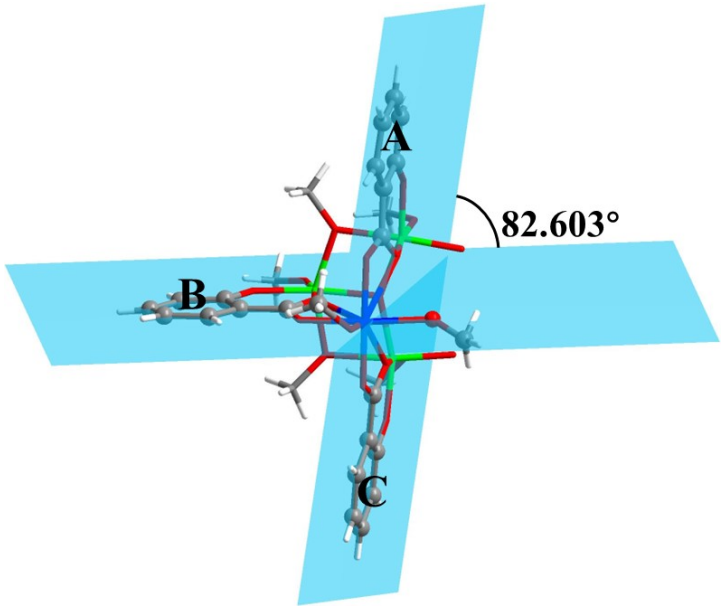

Figure S7. The angle between selected ligands in $\mathbf{(Ti_{10}Cu_2)_{sp}}$.

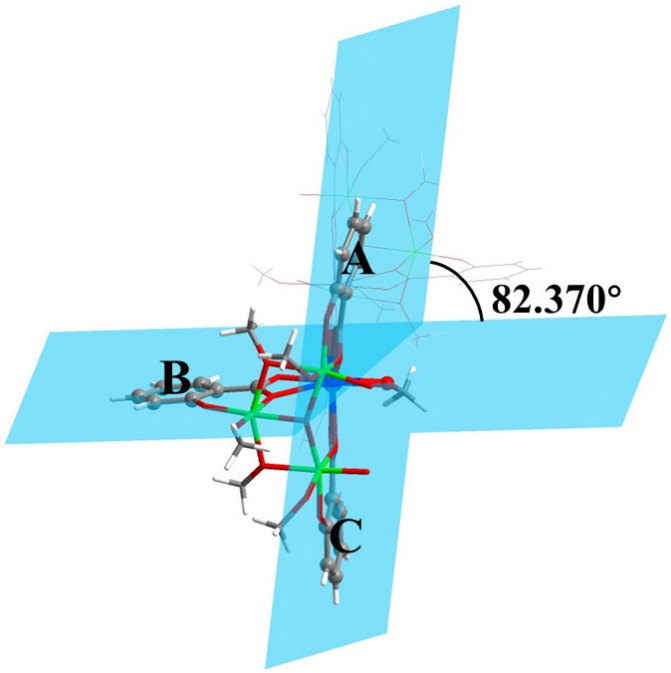

Figure S8. The angle between selected ligands in $(Ti_{10}Cu_2)_{cs}$.

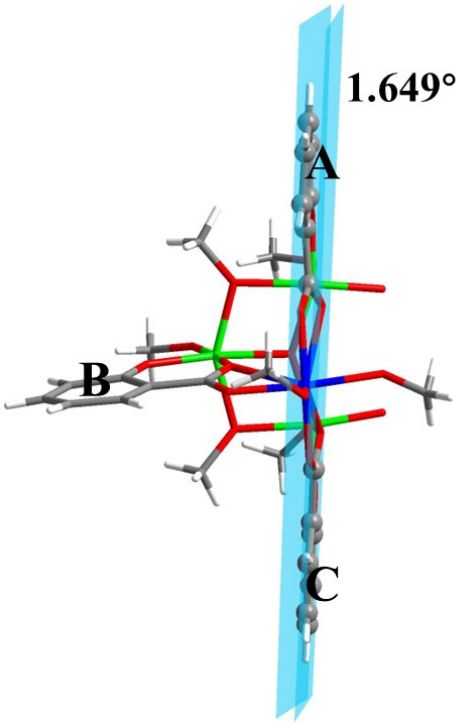

Figure S9. The angle between selected ligands in $(Ti_{10}Cu_2)_{sp}$.

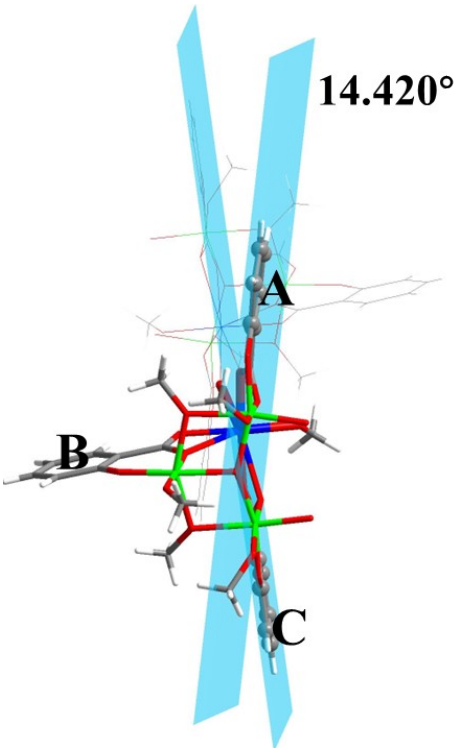

Figure S10. The angle between selected ligands in $(Ti_{10}Cu_2)_{cs}$.

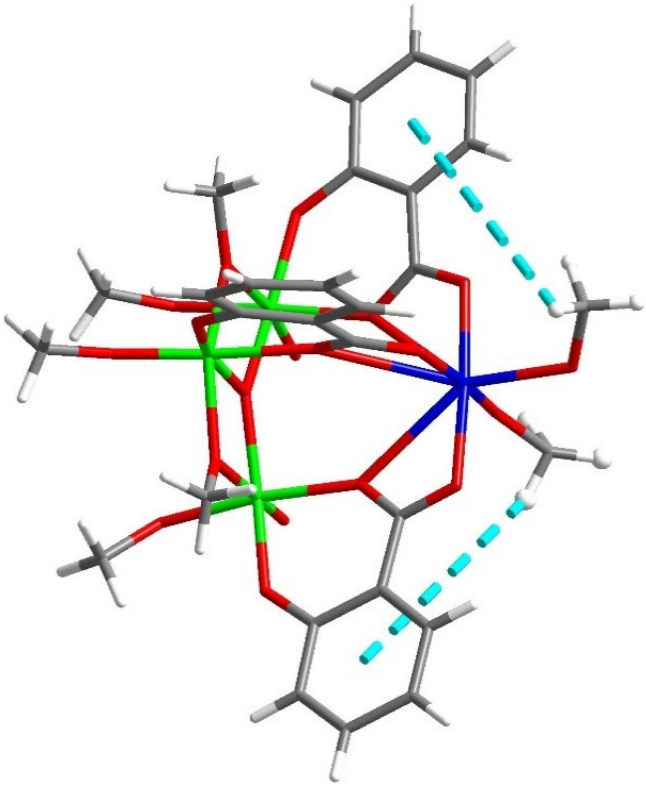

Figure S11. The CH···π interaction in $(Ti_{10}Cu_2)_{sp}$.

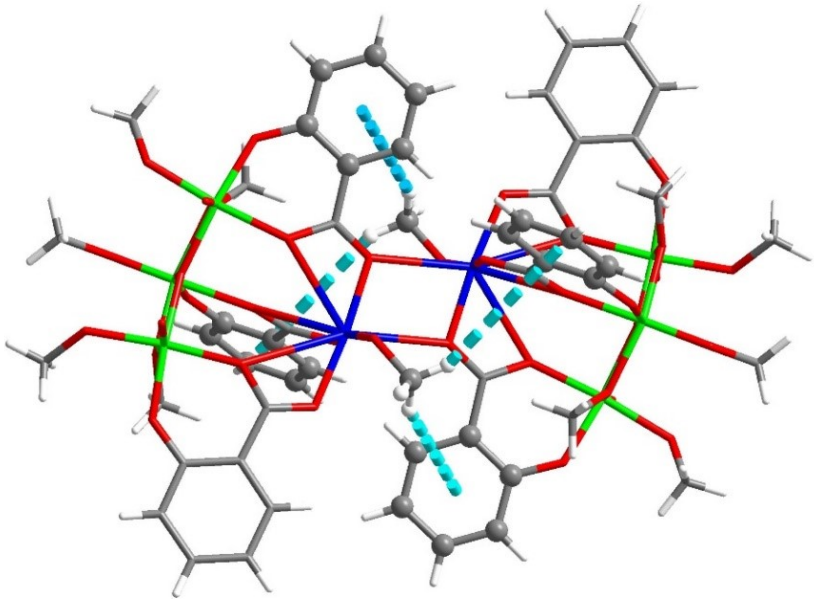

Figure S12. The CH···π interaction in **$(Ti_{10}Cu_2)_{cs}$**.

Table S1. Crystal data and structure refinement for the two compounds.

Compound	**$(Ti_{10}Cu_2)_{sp}$**	**$(Ti_{10}Cu_2)_{cs}$**
Empirical formula	$C_{74}H_{94}Cu_2O_{50}Ti_{10}$	$C_{37}H_{46}CuO_{25}Ti_5$
Formula weight	2389.57	1193.78
Temperature/K	150.0	150.0
Crystal system	monoclinic	monoclinic
Space group	$P2_1/c$	$P2_1/c$
a/Å	16.9694(14)	13.4289(8)
b/Å	20.0230(16)	15.1203(9)
c/Å	15.9095(12)	23.7368(14)
α/°	90	90
β/°	108.640(3)	101.976(2)
γ/°	90	90
Volume/Å^3	5122.1(7)	4714.8(5)
Z	2	4
ρ_{calc}g/cm^3	1.549	1.682
μ/mm^{-1}	1.230	8.138
F(000)	2432.0	2428.0
Crystal size/mm^3	0.11 × 0.1 × 0.09	0.15 × 0.1 × 0.08
Radiation	Mo Kα (λ = 0.71073)	Cu Kα (λ = 1.54178)
2Θ range for data collection/°	4.716 to 55.154	9.132 to 137
Index ranges	$-22 \le h \le 22, -26 \le k \le 26, -19 \le l \le 20$	$-16 \le h \le 16, -17 \le k \le 18, -25 \le l \le 28$
Reflections collected	96590	39028
Independent reflections	11787 [R_{int} = 0.0526, R_{sigma} = 0.0306]	8617 [R_{int} = 0.0445, R_{sigma} = 0.0352]
Data/restraints/parameters	11787/43/639	8617/6/629
Goodness-of-fit on F^2	1.143	1.062
Final R indexes [I>=2σ (I)]	R1 = 0.1058, wR2 = 0.2654	R_1 = 0.0323, wR_2 = 0.0925
Final R indexes [all data]	R1 = 0.1113, wR2 = 0.2684	R_1 = 0.0340, wR_2 = 0.0978
Largest diff. peak/hole / e Å^{-3}	2.57/-2.05	1.28/-0.85

Table S2. Selected bond lengths (Å) and angles (°) for the two compounds.

$(Ti_{10}Cu_2)_{sp}$			
Cu1-O23	2.0694(1)	Cu1-O11	2.1819(1)
Cu1-O9	1.9589(1)	Cu1-O14	2.8603(2)
Cu1-O17	1.9885(1)	Cu1-O15	2.8629(2)
Cu1-O24	2.7397(2)	Cu1-O21	1.9808(1)
Cu1-O23-C38	134.655(5)	Cu1-O11-C33	118.907(5)
$(Ti_{10}Cu_2)_{cs}$			
Cu1-O23	1.9544(1)	Cu1-O19	2.7080(2)
Cu1-O19	1.9785(1)	Cu1-O9	1.9541(1)
Cu1-O21	1.9760(1)	Cu1-O12	2.8028(1)
Cu1-O22	2.8415(1)	Cu1-O14	2.8169(1)
Cu1-O19-C18	142.429(3)	Cu1-O23-C35	121.529(4)

Powder X-ray diffraction (PXRD)

The Powder X-ray diffraction (PXRD) patterns for $(Ti_{10}Cu_2)_{cs}$ and $(Ti_{10}Cu_2)_{sp}$ can be compared with the simulated pattern obtained from the X-ray single-crystal diffraction analysis. Their peak positions are in good agreement with each other, indicating the phase purity of the products. The differences in intensity may be due to the preferred orientation of the powder samples.

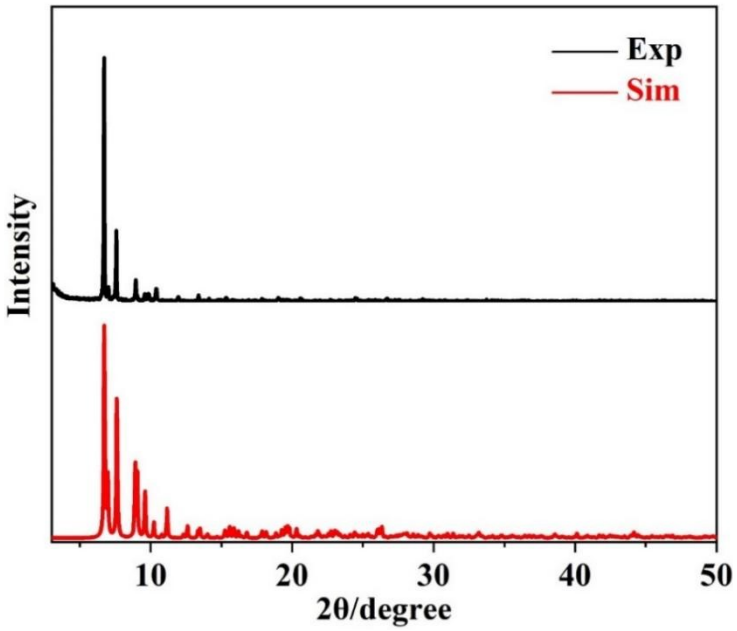

Figure S13. PXRD pattern of $(Ti_{10}Cu_2)_{cs}$.

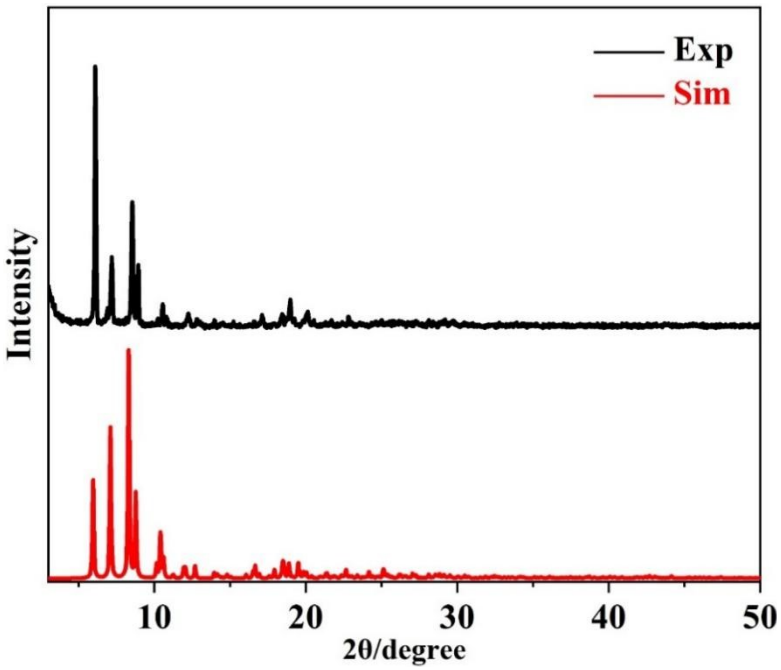

Figure S14. PXRD pattern of $(Ti_{10}Cu_2)_{sp}$.

Fourier Transform Infrared Spectroscopy (FTIR)

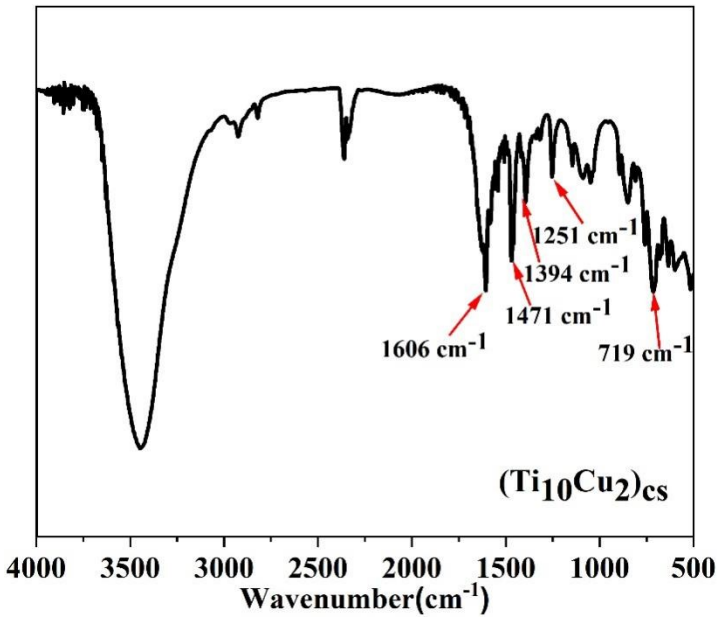

Figure S15. IR spectra of $(Ti_{10}Cu_2)_{cs}$.

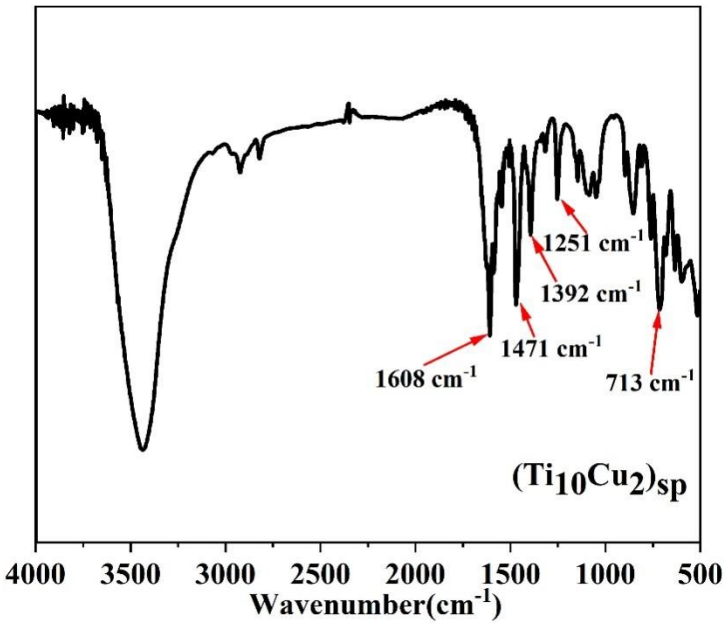

Figure S16. IR spectra of $(Ti_{10}Cu_2)_{sp}$.

Thermogravimetric analyses (TGA)

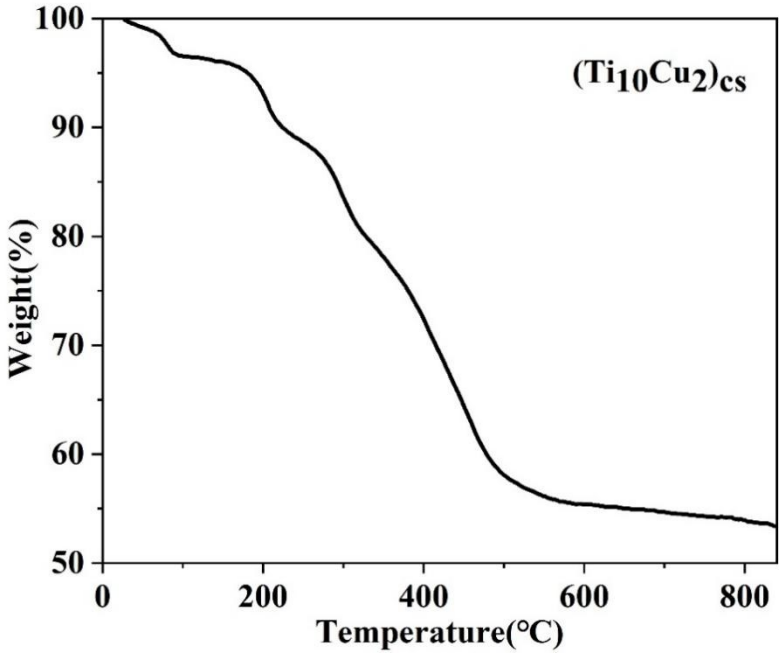

Figure S17. Thermogravimetric analysis trace of $(Ti_{10}Cu_2)_{cs}$.

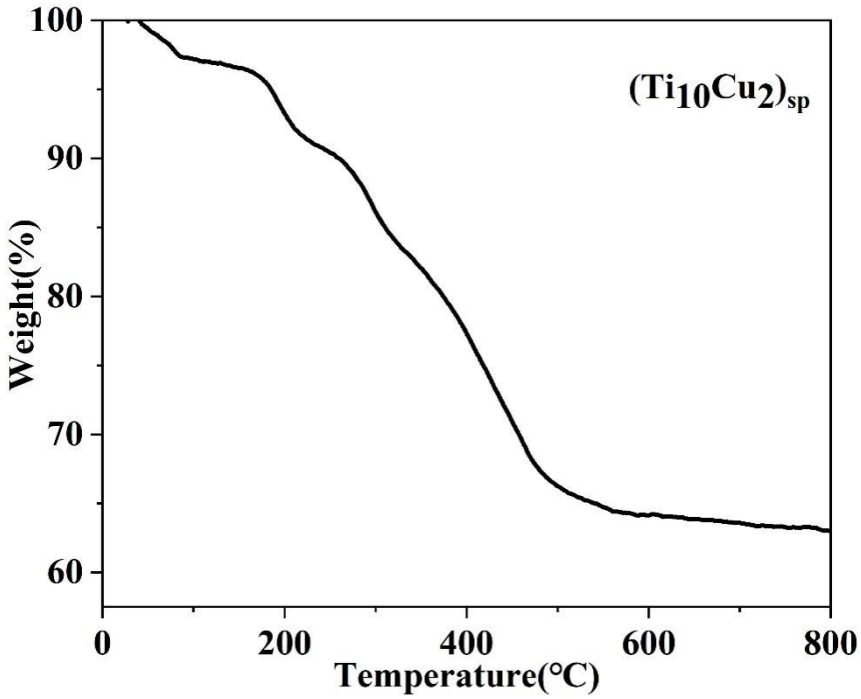

Figure S18. Thermogravimetric analysis trace of $(Ti_{10}Cu_2)_{sp}$.

The thermogravimetric tests with heating rate of 10 ºC / min in nitrogen atmosphere show continuous weight loss from room temperature to 300 ℃,corresponding to the

elimination of coordinated solvent molecules, after which the structures begin thermal decomposition.

UV-Vis absorption spectra (UV)

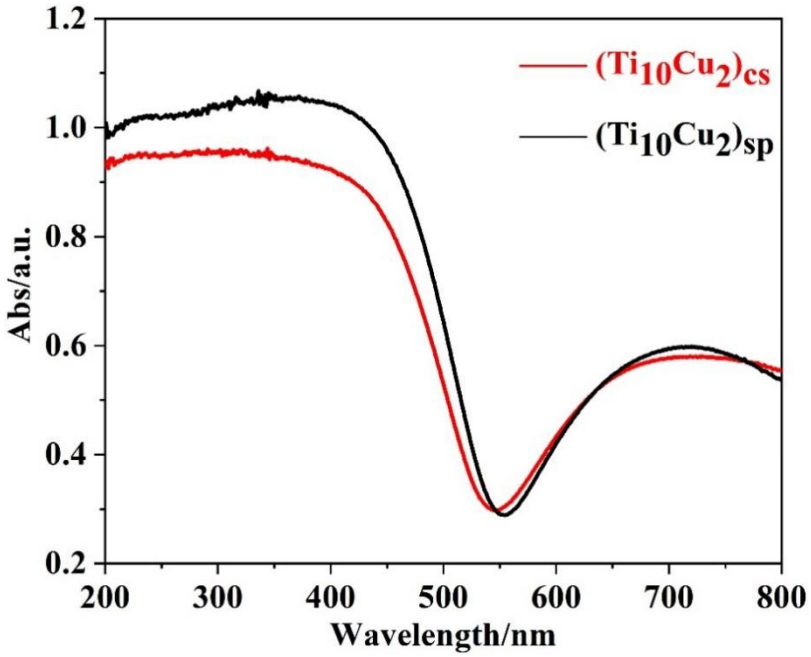

Figure S19. Solid-state UV−vis absorption spectrum of $(Ti_{10}Cu_2)_{sp}$ and $(Ti_{10}Cu_2)_{cs}$.

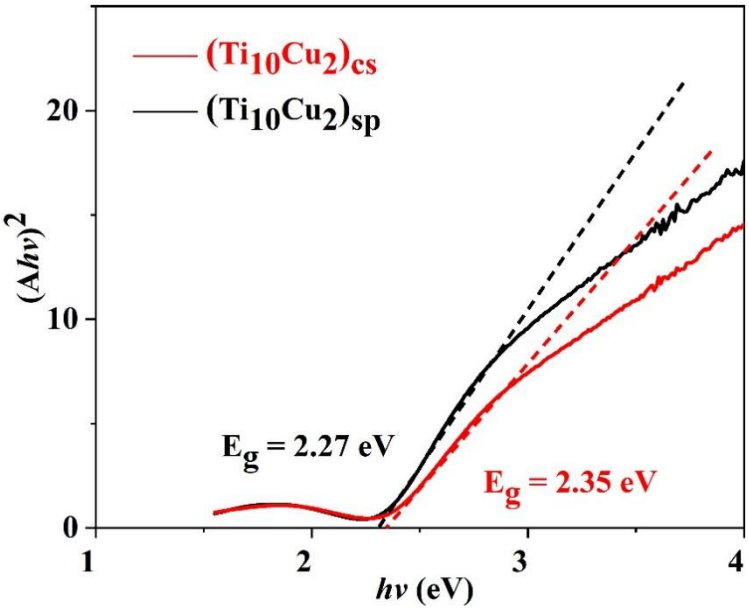

Figure S20. Tauc plots of $(Ti_{10}Cu_2)_{sp}$ and $(Ti_{10}Cu_2)_{cs}$.

Electrochemistry

The electrochemical properties of $\mathbf{(Ti_{10}Cu_2)_{cs}}$ and $\mathbf{(Ti_{10}Cu_2)_{sp}}$ were determined in $CHCl_3$ solution with 0.1M TBA-PF_6. Electrochemical station (CHI 660E, China) was used to perform all the electrochemical experiments at room temperature via the conventional three-electrode electrochemical cell consisting of a platinum wire as the counter electrode, a Ag/AgCl (KCl-saturated) as the reference electrode, and a Glassy carbon electrode as the working electrode. As is shown in Figure S21 and Figure S22, $\mathbf{(Ti_{10}Cu_2)_{cs}}$ displays two pairs of reversible redox peaks in the potential range of 0 V to 1400 mV, these peaks were attributed to the redox process of the Ti^{IV} and Cu^{II} centres. The cyclic voltammetry curves of $\mathbf{(Ti_{10}Cu_2)_{cs}}$ and $\mathbf{(Ti_{10}Cu_2)_{sp}}$ show oxidative peaks at + 0.77 V and + 1.17V, and reductives peak at + 0.67 V and + 1.05 V, which corresponds to the redox couple of Cu(II) and Ti (IV), respectively.

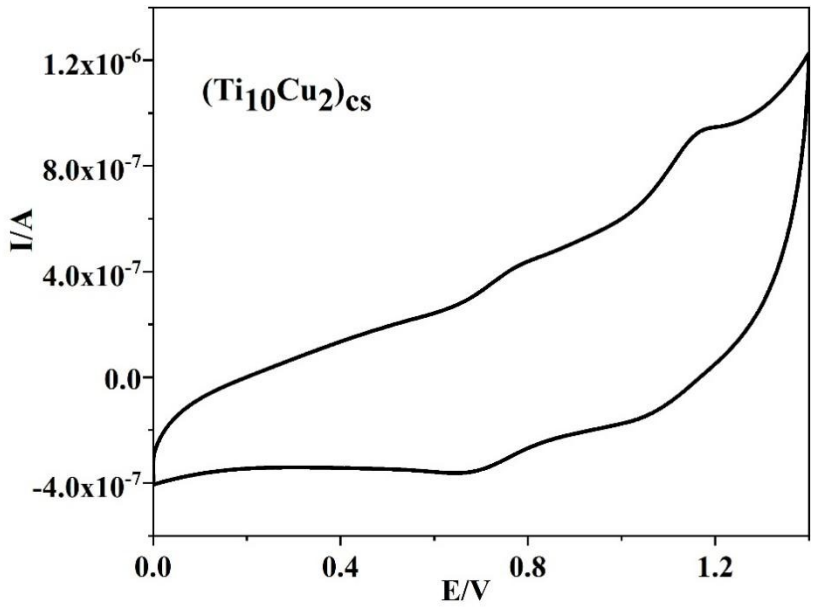

Figure S21. Cyclic voltammogram of $\mathbf{(Ti_{10}Cu_2)_{cs}}$ at a scan rate of 50 mV s^{-1}.

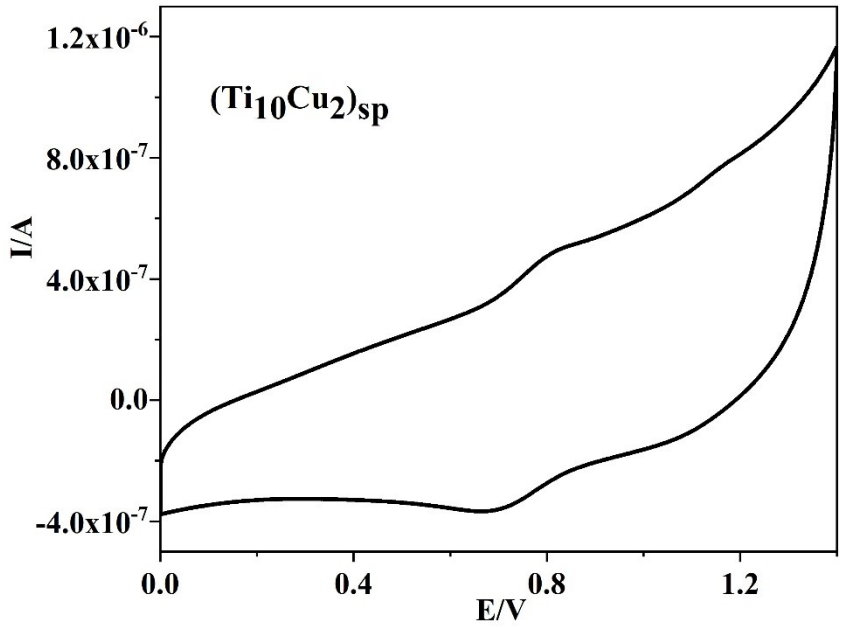

Figure S22. Cyclic voltammogram of $\mathbf{(Ti_{10}Cu_2)_{sp}}$ at a scan rate of 50 mV s^{-1}.

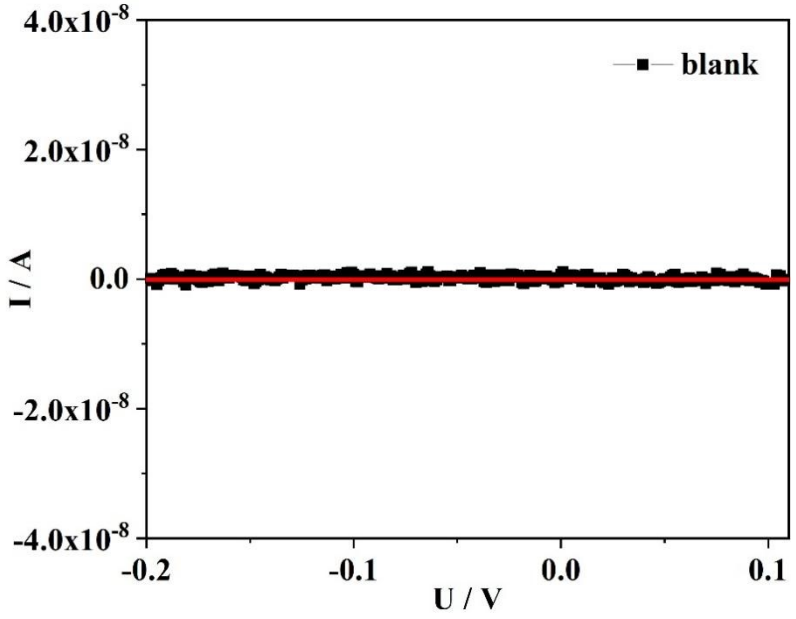

Figure S23. The conductance of blank ranging from -0.2 to 0.2 V.

Photocatalytic CO_2 reductions activity measurement

Photocatalytic reduction of CO_2 was performed in a 250 mL quartz reactor with as-prepared crystal. Photocatalyst (10mg) was added into the mixed solution which contains H_2O (38 mL), acetonitrile (4 mL) and triethanolamine (TEOA, 4 mL) as an electron donor and $[Ru(bpy)_3]Cl_2 \cdot 6H_2O$ as a photosensitizer. After degassing with high-purity CO_2 to remove dissolved O_2 for 30 min. Light source is the xenon (Xe) lamp (300 W, CEL-HXF300-T3, CHINA EDUCATION AU-LIGHT, China). The reaction temperature was controlled at 303 K by using the cooling water circulation. The gas products analyzed by gas chromatograph (FULI GC9790II gas chromatograph, China) with flame ionization detector.

Photoelectrochemical (PEC) measurements were performed on an electrochemical workstation (CHI 660E, China) in a standard three-electrode cell using a Pt wire and an Ag/AgCl electrode (saturated KCl) as the counter and reference electrodes, respectively. The working electrode was prepared on fluorine-doped tin oxide (FTO) glass with its boundary being protected by Scotch tape. The as-synthesized powder (2 mg) was dispersed into 0.4 mL of C_2H_5OH under sonication for 30 min to obtain a colloidal dispersion. The dispersion was drop-casted onto the FTO glass. After natural air drying, the uncoated part of the FTO glass was isolated with epoxy resin glue. Na_2SO_4 aqueous solution (0.2 M, pH = 6.8) was used as an electrolyte. A solar simulator was utilized as a light source for the measurements.

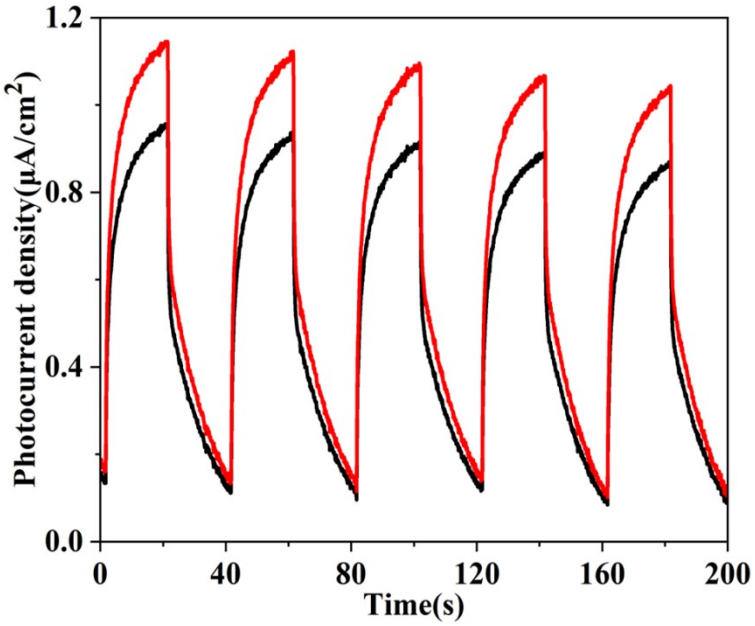

Figure S24. Transient photocurrent response of $\mathbf{(Ti_{10}Cu_2)_{sp}}$ (black) and $\mathbf{(Ti_{10}Cu_2)_{cs}}$ (red).

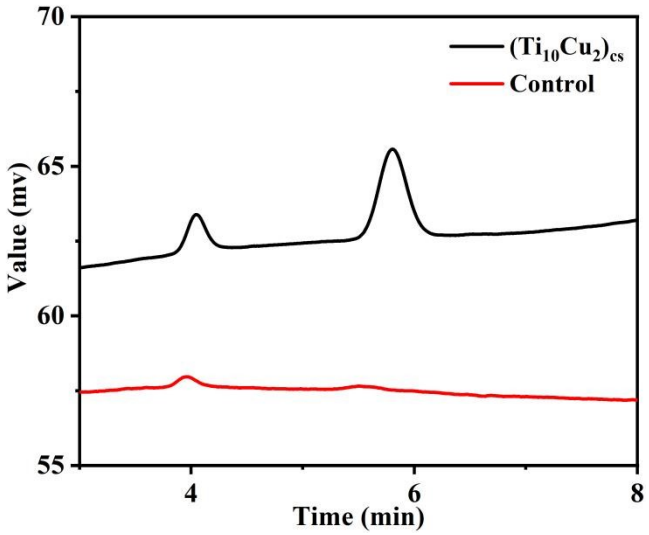

Figure S25. GC analysis of the gaseous reaction products for $(Ti_{10}Cu_2)_{cs}$ (black) and Control Group (no photosensitizer, red) by using the FID. The amount of gas product is calculated from the peak area.

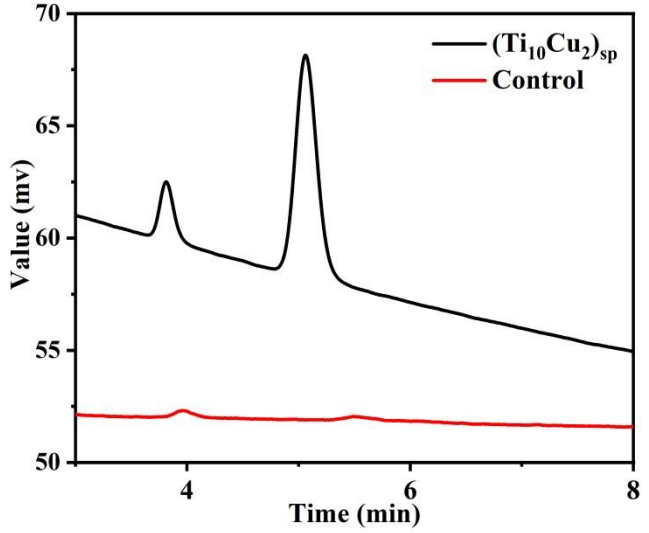

Figure S26. GC analysis of the gaseous reaction products for $(Ti_{10}Cu_2)_{sp}$ (black) and Control Group (no photosensitizer, red) by using the FID. The amount of gas product is calculated from the peak area.

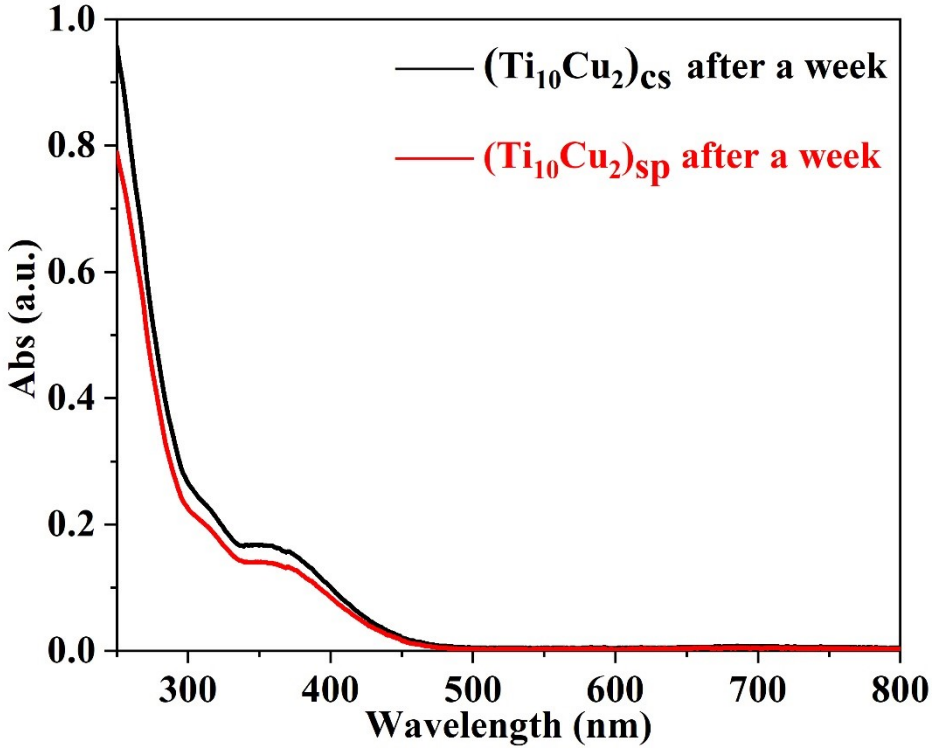

Figure S27. UV spectra of the $(Ti_{10}Cu_2)_{cs}$ and $(Ti_{10}Cu_2)_{sp}$ in chloroform after a week.

Table S3. Comparison of the activity of photocatalytic CO_2 reduction between the catalysts in this work and those reported in the literatures.

Entry	Catalyst	Light source	Sacrificial agent	Product	Activity ($\mu mol \cdot g^{-1} \cdot h^{-1}$)	Refs
1	Cu_2O@Cu@UiO-66-NH_2	300 W Xe lamp	TEOA	CO	20.9	[1]
2	Cu_2O-111-Cu^0	300 W Xe lamp	None	CO	78.4	[2]
3	TiO_2@Bi_2MoO_6	300 W Xe lamp	None	CO	30.6	[3]
4	ZnTCPP/TiO_2	300 W Xe lamp	TEOA	CO	109.33	[4]
				CH_4	9.94	
5	15% P(Cu)/TiO_2	300 W Xe lamp	None	CO	37.21	[5]
6	Bi_2WO_6/TiO_2	Four UV illumination 6 W lamps	None	CH_4	1.06	[6]
7	0.5 Ag-0.5 Cu_2O/TiO_2	300 W Xe lamp	None	CO	13.19	[7]
				CH_4	1.74	
8	NH_2-MIL-125-Ni 1%/Ti	300 W Xe lamp	TEOA	CO	5	[8]
9	NH_2-MIL-125(111)	300 W Xe lamp	TEOA	CO	8.25	[9]
				CH_4	1.01	
10	CuO_x@p-ZnO	300 W Xe lamp	TEA	CO	27.3	[10]
				CH_4	17.9	
				C_2H_4	2.7	
11	Cu NCs@MOF-801	300 W Xe lamp	TEOA	CO	32	[11]
12	$CuCo_2O_4$-400	300 W Xe lamp	TEOA	CO	22.9	[12]
13	Cu/TiO_2	300 W Xe lamp	None	CO	15.27	[13]
14	Cu/CeO_{2-x}	300 W Xe lamp	None	CO	1.65	[14]
15	α-Fe_2O_3/Cu_2O	300 W Xe lamp	None	CO	3.34	[15]
16	33% wtCo-MOF/Cu_2O	300 W Xe lamp	None	CO	3.83	[16]

17	$Cu^{\delta+}/CeO_2$-TiO_2	300 W Xe lamp	None	CO	3.47	[17]
				CH_4	1.52	
				C_2H_4	4.51	
18	Cu/$CsPbBr_3$-Cs_4PbBr_6	300 W Xe lamp	None	CO	14.6	[18]
				CH_4	13.4	
19	SiW_9Ni_4	300 W Xe lamp	TEOA	CO	15.3	[19]
20	Co_{16}-V_4	LED light (λ = 450 nm)	TEOA	CO	1.04	[20]
21	$V_{12}B_{18}$ – Ni	300 W Xe lamp	TEOA	CO	3.2	[21]
22	$(Ti_{10}Cu_2)_{cs}$	300 W Xe lamp	TEOA	CO	24	This work
				CH_4	11	
23	$(Ti_{10}Cu_2)_{sp}$	300 W Xe lamp	TEOA	CH_4	11.5	This work

TEOA: Triethanolamine, TEA: Triethylamine, TIPA: Triisopropanolamine.

Reference:

1. S. Q. Wang; X. Y. Zhang; X. Y. Dao; X. M. Cheng; W. Y. Sun, Cu_2O@Cu@UIO-66-NH_2 ternary nanocubes for photocatalytic CO_2 reduction. *ACS Appl. Nano Mater.* **2020,** *3*, 10437.
2. Y. Deng; C. Wan; C. Li; Y. Y. Wang; X. Y. Mu; W. Liu; Y. P. Huang; P. K. Wong; L. Q. Ye, Synergy effect between facet and zero-valent copper for selectivity photocatalytic methane formation from CO_2. *ACS Catal.* **2022,** *12*, 4526.
3. G. M. Ren; Z. X. Wei; Z. Z. Li; X. C. Zhang; X. C. Meng, Fabrication of S-scheme hollow TiO_2@Bi_2MoO_6 composite for efficiently photocatalytic CO_2 reduction. *Mater. Today Chem.* **2023,** *27*, 101260.
4. A. Li; S. Y. Chen; F. C. Yang; H. Y. Gao; C. Dong; G. Wang, Metalloporphyrin-decorated titanium dioxide nanosheets for efficient photocatalytic carbon dioxide reduction. *Inorg. Chem.* **2021,** *60*, 18337.
5. L. Wang; P. X. Jin; J. W. Huang; H. D. She; Q. Z. Wang, Integration of copper(II)-porphyrin zirconium metal–organic framework and titanium dioxide to construct Z-Scheme system for highly improved photocatalytic CO_2 reduction. *ACS Sustainable Chem. Eng.* **2019,** *7*, 15660.
6. L. Collado; M. Gomez Mendoza; M. García-Tecedor; F. E. Oropeza; A. Reynal; J. R. Durrant; D. P. Serrano; V. A. de la Peña O'Shea, Towards the improvement of methane production in CO_2 photoreduction using Bi_2WO_6/TiO_2 heterostructures. *Appl. Catal., B* **2023,** *324*, 122206.
7. X. N. Wang; Z. L. Jiang; H. W. Chen; K. Wang; X. T. Wang, Photocatalytic CO_2 reduction with water vapor to CO and CH_4 in a recirculation reactor by Ag-Cu_2O/TiO_2 Z-Scheme heterostructures. *J. Alloys Compd.* **2022,** *896*, 163030.
8. S. Y. Chen; G. T. Hai; H. Y. Gao; X. Chen; A. Li; X. W. Zhang; W. J. Dong, Modulation of the charge transfer behavior of Ni(II)-doped NH_2-MIL-125(Ti): Regulation of ni ions content and enhanced photocatalytic CO_2 reduction performance. *Chem. Eng. J.* **2021,** *406*, 126886.
9. X. M. Cheng; X. Y. Dao; S. Q. Wang; J. Zhao; W. Y. Sun, Enhanced photocatalytic CO_2 reduction activity over NH_2-MIL-125(Ti) by facet regulation. *ACS Catal.* **2021,** *11*, 650.
10. W. Wang; C. Y. Deng; S. J. Xie; Y. F. Li; W. Y. Zhang; H. Sheng; C. C. Chen; J. C. Zhao, Photocatalytic C–C coupling from carbon dioxide reduction on copper oxide with mixed-valence copper(I)/copper(II). *J. Am. Chem. Soc.* **2021,** *143*, 2984.
11. S. Dai; T. Kajiwara; M. Ikeda; I. Romero-Muñiz; G. Patriarche; A. E. Platero-Prats; A. Vimont; M. Daturi; A. Tissot; Q. Xu; C. Serre, Ultrasmall copper nanoclusters in zirconium metal-organic frameworks for the photoreduction of CO_2. *Angew. Chem. Int. Ed.* **2022,** *61*, e202211848.
12. M. Jiang; Y. Gao; Z. Y. Wang; Z. X. Ding, Photocatalytic CO_2 reduction promoted by a $CuCo_2O_4$ cocatalyst with homogeneous and heterogeneous light harvesters. *Appl. Catal., B* **2016,** *198*, 180.
13. K. N. Zhu; Q. Zhu; M. P. Jiang; Y. W. Zhang; Z. Y. Shao; Z. B. Geng; X. Y. Wang; H. Zeng; X. F. Wu; W. Zhang; K. K. Huang; S. H. Feng, Modulating Ti t_{2g}

orbital occupancy in a Cu/TiO_2 composite for selective photocatalytic CO_2 reduction to CO. *Angew. Chem. Int. Ed.* **2022,** *61*, e202207600.
14. M. Wang; M. Shen; X. X. Jin; J. J. Tian; M. L. Li; Y. J. Zhou; L. X. Zhang; Y. S. Li; J. L. Shi, Oxygen vacancy generation and stabilization in CeO_{2-x} by Cu introduction with improved CO_2 photocatalytic reduction activity. *ACS Catal.* **2019,** *9*, 4573.
15. J. C. Wang; L. Zhang; W. X. Fang; J. Ren; Y. Y. Li; H. C. Yao; J. S. Wang; Z. J. Li, Enhanced photoreduction CO_2 activity over direct z-scheme α-Fe_2O_3/Cu_2O heterostructures under visible light irradiation. *ACS Appl. Mater. Interfaces* **2015,** *7*, 8631.
16. W. W. Dong; J. Jia; Y. Wang; J. R. An; O. Y. Yang; X. J. Gao; Y. L. Liu; J. Zhao; D. S. Li, Visible-light-driven solvent-free photocatalytic CO_2 reduction to CO by Co-MOF/Cu_2O heterojunction with superior selectivity. *Chem. Eng. J.* **2022,** *438*, 135622.
17. T. Wang; L. A. Chen; C. Chen; M. T. Huang; Y. J. Huang; S. J. Liu; B. X. Li, Engineering catalytic interfaces in $Cu^{\delta+}$/CeO_2-TiO_2 photocatalysts for synergistically boosting CO_2 reduction to ethylene. *ACS Nano* **2022,** *16*, 2306.
18. L. J. Li; Z. H. Zhang, In-situ fabrication of Cu doped dual-phase $CsPbBr_3$–Cs_4PbBr_6 inorganic perovskite nanocomposites for efficient and selective photocatalytic CO_2 reduction. *Chem. Eng. J.* **2022,** *434*, 134811.
19. Q. Chang; X. Y. Meng; W. J. Ruan; Y. Q. Feng; R. Li; J. Y. Zhu; Y. Ding; H. J. Lv; W. Wang; G. Y. Chen; X. K. Fang, Metal-organic cages with {SiW_9Ni_4} polyoxotungstate nodes. *Angew. Chem. Int. Ed.* **2022,** *61*, e202117637.
20. L. Z. Qiao; M. Song; A. F. Geng; S. Yao, Polyoxometalate-based high-nuclear cobalt–vanadium–oxo cluster as efficient catalyst for visible light-driven CO_2 reduction. *Chin. Chem. Lett.* **2019,** *30*, 1273.
21. X. Yu; C. C. Zhao; J. X. Gu; C. Y. Sun; H. Y. Zheng; L. K. Yan; M. Sun; X. L. Wang; Z. M. Su, Transition-metal-modified vanadoborate clusters as stable and efficient photocatalysts for CO_2 reduction. *Inorg. Chem.* **2021,** *60*, 7364.